

OPEN ACCESS


Annealing Effects on the Band Alignment of ALD SiO₂ on (In_xGa_{1-x})₂O₃ for x = 0.25–0.74

To cite this article: Chaker Fares *et al* 2020 *ECS J. Solid State Sci. Technol.* **9** 045001

View the [article online](#) for updates and enhancements.



Annealing Effects on the Band Alignment of ALD SiO₂ on (In_xGa_{1-x})₂O₃ for x = 0.25–0.74

Chaker Fares,^{1,*} Minghan Xian,¹ David J. Smith,² M. R. McCartney,² Max Kneiß,³ Holger von Wenckstern,³ Marius Grundmann,³ Marko Tadjer,⁴ Fan Ren,^{1,**} and S. J. Pearton^{5,**,z} 

¹Department of Chemical Engineering, University of Florida, Gainesville, Florida 32611, United States of America

²Department of Physics, Arizona State University, Tempe, Arizona 85287, United States of America

³Universität Leipzig, Felix-Bloch-Institut für Festkörperphysik, 04103 Leipzig, Germany

⁴US Naval Research Laboratory, Washington, DC 20375, United States of America

⁵Department of Materials Science and Engineering, University of Florida, Gainesville, Florida 32611, United States of America

The band alignment of Atomic Layer Deposited SiO₂ on (In_xGa_{1-x})₂O₃ at varying indium concentrations is reported before and after annealing at 450 °C and 600 °C to simulate potential processing steps during device fabrication and to determine the thermal stability of MOS structures in high-temperature applications. At all indium concentrations studied, the valence band offsets (VBO) showed a nearly constant decrease as a result of 450 °C annealing. The decrease in VBO was −0.35 eV for (In_{0.25}Ga_{0.75})₂O₃, −0.45 eV for (In_{0.42}Ga_{0.58})₂O₃, −0.40 eV for (In_{0.60}Ga_{0.40})₂O₃, and −0.35 eV (In_{0.74}Ga_{0.26})₂O₃ for 450 °C annealing. After annealing at 600 °C, the band alignment remained stable, with <0.1 eV changes for all structures examined, compared to the offsets after the 450 °C anneal. The band offset shifts after annealing are likely due to changes in bonding at the heterointerface. Even after annealing up to 600 °C, the band alignment remains type I (nested gap) for all indium compositions of (In_xGa_{1-x})₂O₃ studied.

© 2020 The Author(s). Published on behalf of The Electrochemical Society by IOP Publishing Limited. This is an open access article distributed under the terms of the Creative Commons Attribution 4.0 License (CC BY, <http://creativecommons.org/licenses/by/4.0/>), which permits unrestricted reuse of the work in any medium, provided the original work is properly cited. [DOI: 10.1149/2162-8777/ab8364]



Manuscript submitted January 28, 2020; revised manuscript received March 18, 2020. Published April 6, 2020. *This paper is part of the JSS Focus Issue on Gallium Oxide Based Materials and Devices II.*

Besides β-Ga₂O₃'s ultra-wide band gap (4.6–4.8 eV) and high theoretical breakdown field, alloying with Al or In can be used to tune this band gap to be larger or smaller and thereby form heterostructures.^{1–6} Over the range of alloy compositions reported in the literature, this allows realization of bandgaps between ~3.9–5.9 eV, as shown in Fig. 1.^{3,5–11} In order to grow (In_xGa_{1-x})₂O₃, various methods have been reported, such as pulsed laser deposition (PLD), sputtering, molecular beam epitaxy, organic chemical vapor deposition, and sol-gel processing.^{7,12–22} Most of the previous research has focused on native defect behavior, miscibility gaps, and crystal phase structure as the cubic phase of In₂O₃ is alloyed with monoclinic Ga₂O₃.^{7,12–15,23–32} In device applications, the (In_xGa_{1-x})₂O₃ layers can be used as channels in heterostructure transistors and also to tune the wavelength response of photodetectors.^{7,13,15,17,26,29}

For heterostructure transistors to operate with a low gate leakage current, thin dielectric layers can be deposited prior to gate formation to form a metal-oxide-semiconductor (MOS) structure. There are many possible dielectrics one can choose, however, the dielectric's band gap must be large enough such that it offsets the (Al_xGa_{1-x})₂O₃/(In_xGa_{1-x})₂O₃ by ideally >1 eV on both the conduction band and valence band.^{33,34} Another application for these dielectrics is as a passivation layer to prevent surface conductivity changes common to electronic oxides exposed to humid ambient conditions. Atomic layer deposited SiO₂ is one of the most common dielectrics for these applications due to its large band gap and well-established deposition conditions.^{34–37} Another benefit of SiO₂ is that has been shown to be a thermally stable dielectric on Ga₂O₃ up to 1000 °C.^{31,38} By sharp contrast, the Al₂O₃–Ga₂O₃ phase system does not possess the same thermal stability as SiO₂.^{7,8}

Understanding a dielectric's thermal stability on (In_xGa_{1-x})₂O₃ based devices is useful for several applications. During device processing, it is necessary to anneal the structures at temperatures

between 500 °C and 600 °C to form Ohmic contacts.^{39,40} Additionally, if ion implantation is utilized for device isolation in (In_xGa_{1-x})₂O₃ based systems, annealing will be required to optimize sheet resistance. After the devices have been fabricated, the junction temperature of Ga₂O₃ based devices can see large temperature swings under high-current operation due to the marginal thermal conductivity of Ga₂O₃.^{41,40,42,43} Thus far, there have been no reports on how high temperatures affect the band offset between SiO₂ and (In_xGa_{1-x})₂O₃. There have been a few previous studies done examining the annealing effects of dielectrics or other semiconductors on Ga₂O₃ and (Al_xGa_{1-x})₂O₃,^{44–50} but no work has been done on (In_xGa_{1-x})₂O₃ based systems. Yadav et al.⁴⁵ found that the valence band offset between Ga₂O₃ and Si increased with annealing at 600 °C. In general, annealing of dielectrics on other semiconductors such as Si, SiC and InGaAs leads to changes in band offsets due

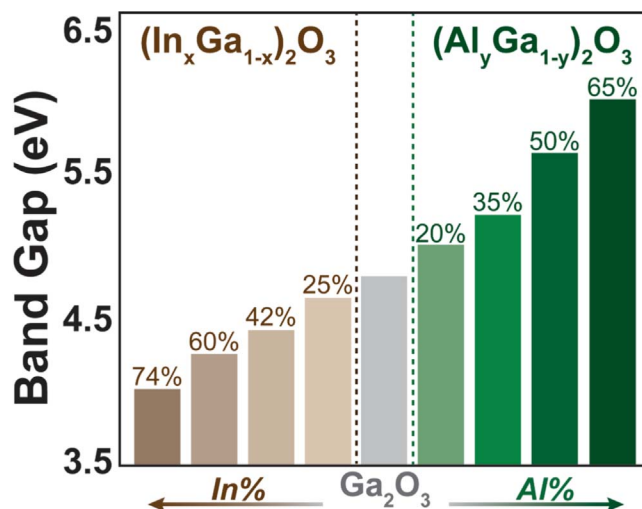


Figure 1. Band gap tunability of Ga₂O₃ by incorporating In or Al to form ternary alloys.

*Electrochemical Society Student Member.

**Electrochemical Society Fellow.

^zE-mail: spear@mse.ufl.edu

to formation of interfacial layers.^{46–50} In this study, we report the effects of post-deposition annealing at 450 °C and 600 °C on the band alignment of ALD SiO₂ on (In_xGa_{1-x})₂O₃. We should point out that we are only examining the change in band alignment and not the important issue of changes in interface state density as a result of this annealing. For example, the diffusion of Indium at high annealing temperature has been addressed as a critical problem which degrades the interface quality of oxide/high k MOS structures.⁵¹ Our structures are thin and undoped and not amenable to capacitance-voltage measurements for obtaining the interface state density, which obviously important in actual device structures and should be the focus of future studies.

Experimental

Continuous composition spread Pulsed Laser Deposition (CCS-PLD) was used to grow (In_xGa_{1-x})₂O₃ from segmented targets of Ga₂O₃ and In₂O₃ targets onto a 2-inch Magnesium Oxide substrate.^{7,19,21,22,26,52–54} The indium concentration was varied from 16% incorporation to over 86% incorporation along the length of the wafer. The oxygen pressure in the growth chamber was 0.08 mbar and the temperature was 650 °C. The measured In concentration followed an S-shaped profile along the length of the sample, which corroborates previous theoretical calculations.²⁰ During previous studies focused on growth optimization, the composition of the

In incorporation across the wafers was verified using Energy-Dispersive X-ray spectroscopy (EDX).^{20,26} The concentration of In was found to be uniform along the perpendicular direction of the growth gradient. The (111) oriented cubic bixbyite phase is dominant for the In-rich portion of the wafer, while the monoclinic phase is dominant for the Ga-rich compositions.¹² After the (In_xGa_{1-x})₂O₃ films were grown, the wafer was diced into smaller pieces in order to study specific compositions of the film. The In compositions used in this work were 25, 42, 60, and 74%. These compositions were determined and verified using the EDX growth map along with X-ray Photoelectron Spectroscopy (XPS). Once the compositions of interest were located on the samples, alignments marks were placed in order to mark exact measurement locations for XPS measurements before and after annealing XPS measurements were taken at three points at each composition of interest to ensure the band alignment did not vary spatially due to potential phase or compositional differences. Uncertainty in spatial variation is less than 50 μm after dicing, which corresponds to a possible compositional variation of ±2% for all structures examined. The bandgap was measured for each sample and was 4.55 eV for (In_{0.25}Ga_{0.75})₂O₃, 4.35 eV for (In_{0.42}Ga_{0.58})₂O₃, 4.2 eV for (In_{0.60}Ga_{0.40})₂O₃, and 4.05 eV for (In_{0.74}Ga_{0.26})₂O₃. Further details can be found elsewhere.⁵⁵

Prior to dielectric deposition onto the (In_xGa_{1-x})₂O₃ samples, acetone and isopropyl alcohol rinses were used to clean the wafer

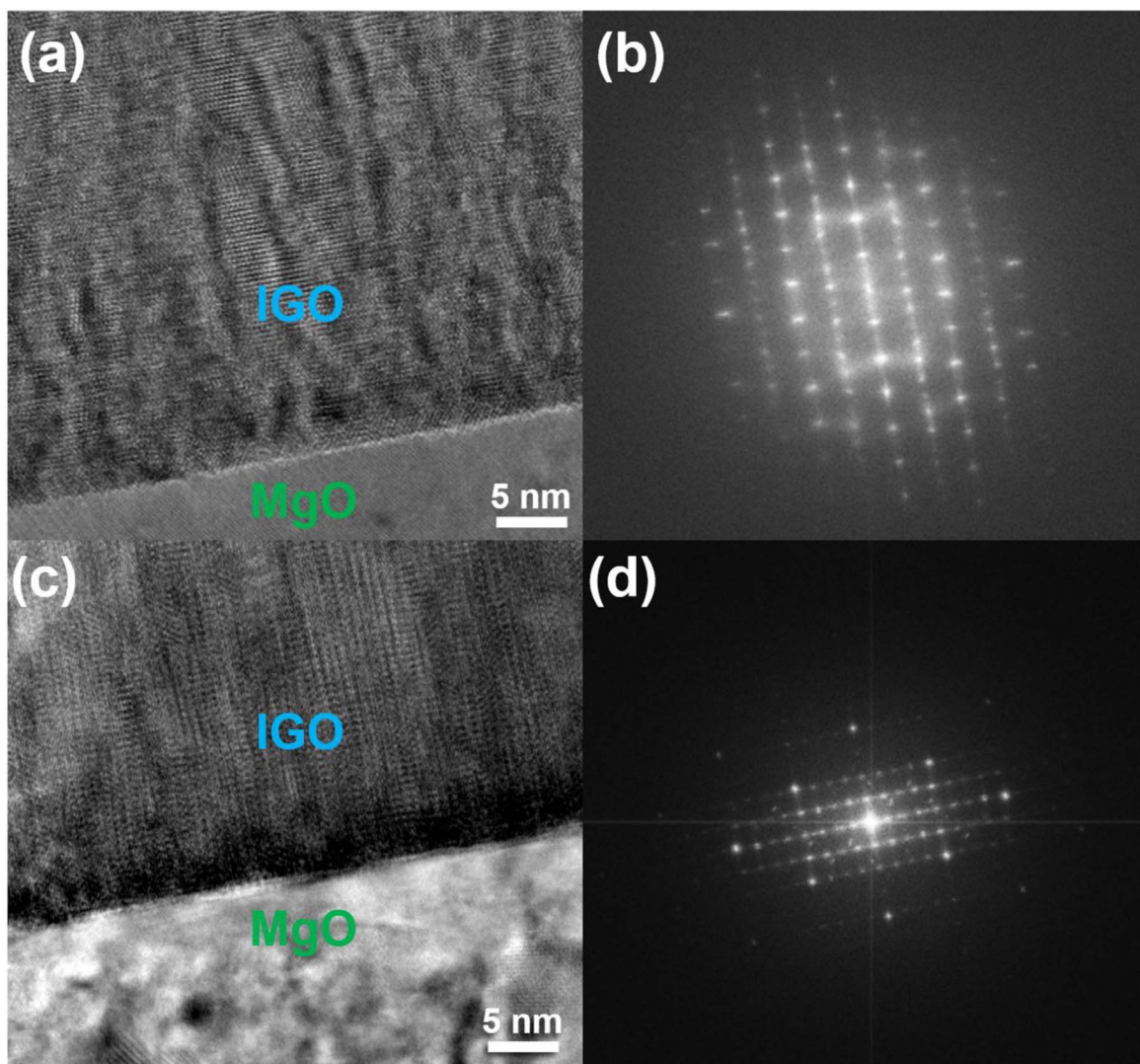


Figure 2. High-resolution TEM images and corresponding fast Fourier transforms (FFT) from (a)–(b) the bottom of the gallium-rich portion and (c)–(d) the bottom of the indium-rich portion of the (In_xGa_{1-x})₂O₃ wafer.

surface. After solvent cleaning, dry N_2 gas was used to dry the samples which were subsequently exposed to ozone for 15 min to remove residual carbon contamination. After cleaning, the IGO pieces were loaded into the Atomic Layer Deposition chamber located in a cleanroom. The deposition temperature of the SiO_2 was 200 °C in a Cambridge Nano Fiji 200 using a remote plasma mode. A thin (1.5 nm) layer of SiO_2 was deposited onto the $(In_xGa_{1-x})_2O_3$ samples to measure the band alignment within the heterostructure. Thick (200 nm) layers of SiO_2 were deposited as a reference to measure the dielectric's core levels and its respective bandgap. The ALD precursors for the SiO_2 deposition were a Tris (dimethylamino) silane and a 300 W inductively coupled plasma (ICP) to generate atomic oxygen.^{35,55,56}

A rapid thermal annealing system was utilized to anneal the $SiO_2/(In_xGa_{1-x})_2O_3$ heterostructures at 450 °C and 600 °C under N_2 ambient for 5 min. The band alignment of the heterostructures was measured as deposited and after each annealing cycle. The annealing temperatures were chosen to replicate potential device processing steps for IGO based device fabrication. The two separate temperature anneals were performed to examine the thermal stability of the heterostructure band alignment.

For the XPS measurements, a Physical Instruments ULVAC PHI system was utilized. The XPS system operated using a monochromatic Al X-ray source (1486 eV, source power 300 W) at a take-off angle of 50°, acceptance angle of 7°, and analysis area of 100 μm in diameter. XPS survey scans were used to verify the SiO_2 , $(In_xGa_{1-x})_2O_3$, and heterostructures of the two were free from impurities and contamination.⁵⁷ The electron pass energy was 93.5 eV for survey scans and 23.5 eV for high-resolution scans. The energy resolution of the XPS system was approximately 0.5 eV and binding energy accuracy was within 0.03 eV. The C 1s core level of adventitious carbon (284.8 eV) was used to calibrate the binding energy on all samples. Binding energy calibration plays no effect on the final band alignment values since the offsets are determined using only relative energy positions. To avoid sample charging during the measurements, an electron flood gun and ion beam were used simultaneously. To prevent uneven charge dissipation from the samples to the chuck, the samples were electronically insulated from the platen. The bandgap of the ALD deposited SiO_2 was measured using Reflection Electron Energy Loss Spectroscopy (REELS) utilizing a 1 kV electron beam and hemispherical analyzer.

An aberration-corrected FEI Titan 80–300 electron microscope operated at 300 kV was used to record TEM images of the $(In_xGa_{1-x})_2O_3$ films. Samples were prepared for cross-sectional observation using an FEI Nova 200 focused-ion-beam system.

Results and Discussion

The $SiO_2/(In_xGa_{1-x})_2O_3$ samples were examined before and after annealing by TEM to study the effect of In concentration on the IGO's crystal structure and uniformity. Figure 2 shows high-resolution TEM images and corresponding fast Fourier transforms (FFT) from (a–b) the bottom of the gallium-rich portion and (c–d) the bottom of the indium-rich portion of the $(In_xGa_{1-x})_2O_3$ film. The TEM and FFT photos indicate that the IGO sample is crystalline in nature for both the gallium rich and indium rich portions of the wafer. No threading dislocations or major defects in the crystal structure are detected for the studied compositions of $(In_xGa_{1-x})_2O_3$. The $(In_xGa_{1-x})_2O_3$ growth is primarily normal and parallel to the MgO substrate. When observing the FFTs of the indium and gallium rich portions of the $(In_xGa_{1-x})_2O_3$, there are clear crystallographic differences. Two main phases are present, namely the monoclinic phase of β - Ga_2O_3 and the cubic phase of bixbyite In_2O_3 , which agrees with previously taken XRD measurements.^{12,22} The indium-rich portion of the film shows columnar grains extending through the film but is still crystalline and epitaxial with regards to the MgO substrate. In a previous TEM analysis of various regions of the IGO film, the presence of grain boundaries became evident towards the upper portion of the deposited In-rich film. The Ga-rich portion

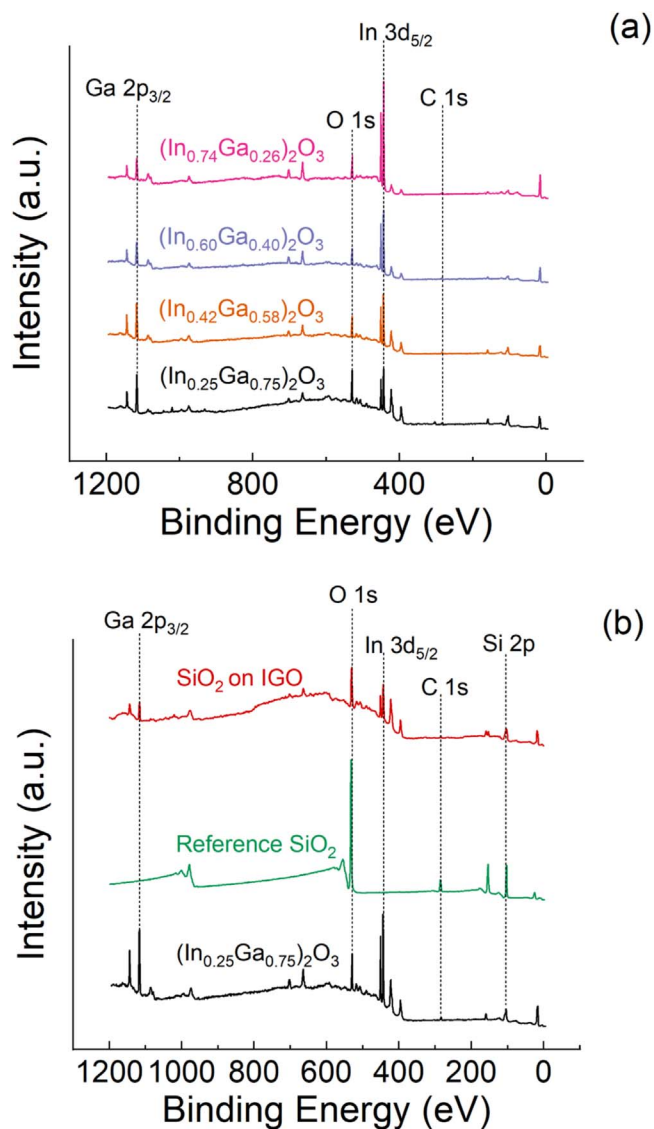


Figure 3. XPS survey scans of (a) $(In_xGa_{1-x})_2O_3$ at the aluminum concentrations studied and (b) thick ALD SiO_2 and its heterostructure on IGO. The intensity is in arbitrary units (a.u.).

shows homogenous growth throughout the entire thickness of the film. At higher In compositions than those studied in this report, the rhombohedral $InGaO_3$ (II) phase was also present. The extent of phase separation significantly decreases as the In concentration is reduced.

XPS survey scans were taken on the $(In_xGa_{1-x})_2O_3$ samples at each In concentration, the reference bulk ALD SiO_2 , and the SiO_2/IGO heterostructures. Figure 3 shows that only lattice constituents are present in the survey scans and no contamination is detectable for any of the samples. The bandgap of the ALD deposited SiO_2 was measured to be 8.7 eV using Reflection Electron Energy Loss Spectroscopy (REELS), which is similar to previous reports.^{34,58}

High resolution XPS spectra for the as-deposited $(In_xGa_{1-x})_2O_3$ to SiO_2 core delta regions are shown in Figs. 4a, 4b. After these measurements were taken, the $SiO_2/(In_xGa_{1-x})_2O_3$ heterostructures along with reference SiO_2 and bulk ALD deposited SiO_2 were annealed at 450 °C for 5 min in N_2 ambient. High resolution XPS measurements were repeated after 450 °C annealing of the same heterostructure core delta regions and are shown in Figs. 4c, 4d. A final anneal at 600 °C was performed and post-anneal XPS data is shown in Figs. 4e, 4f. After annealing, peak broadening is evident in

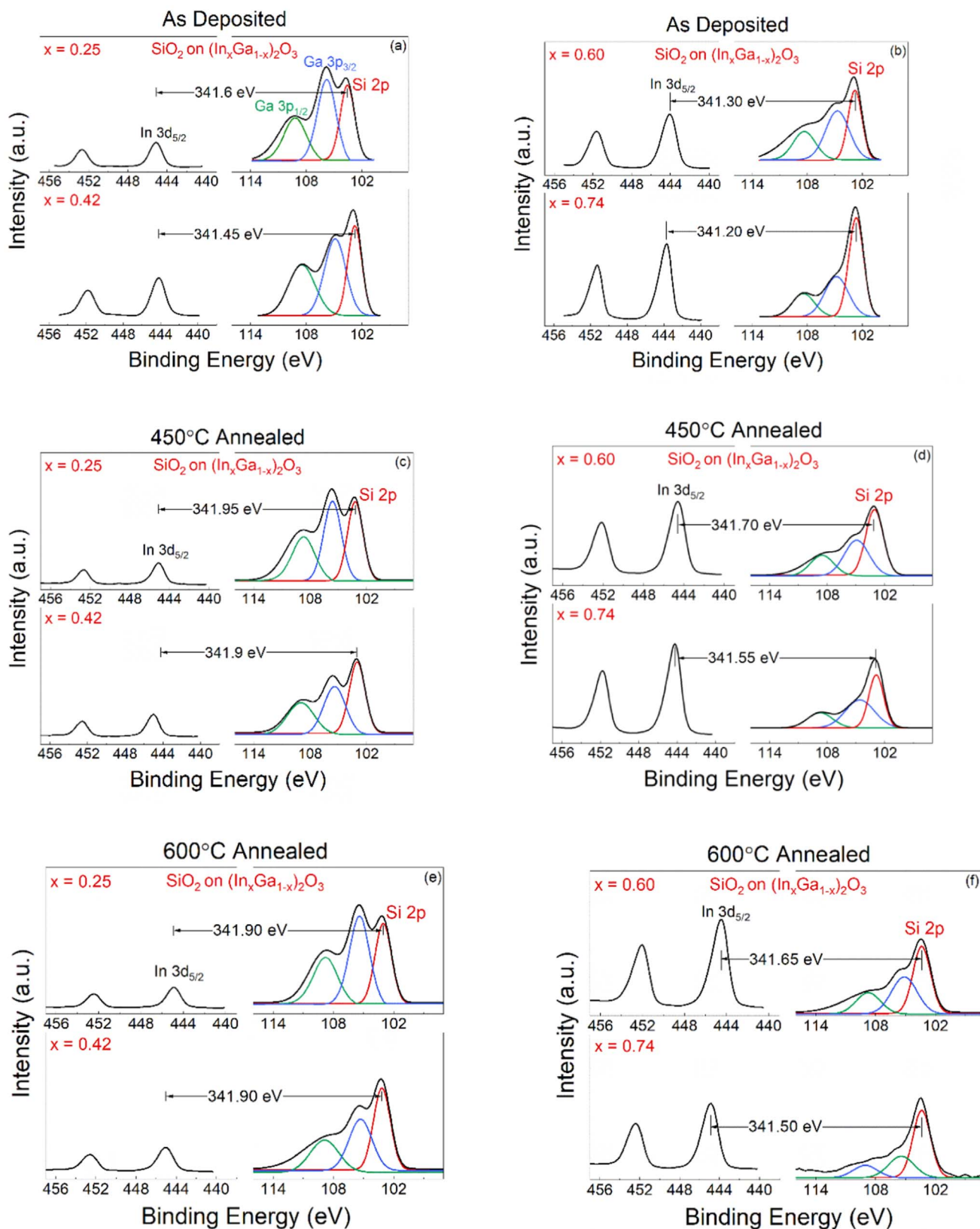


Figure 4. High resolution XPS spectra for the (a)–(b.) $(\text{In}_x\text{Ga}_{1-x})_2\text{O}_3$ to SiO_2 core delta regions as deposited, (c)–(d.) after annealing at 450 °C for 5 min in N_2 ambient, and (e)–(f.) after annealing at 600 °C for 5 min in N_2 ambient. The intensity is in arbitrary units (a.u.).

the $\text{Ga}3p_{1/2}$, $\text{Ga}3p_{3/2}$, and $\text{Si}2p$ peak locations. This is most likely due to disorder and non-uniformities causing an energy distribution broadening of the orbitals of interest. Additionally, Fig. 4 shows that

annealing causes the diversification of various Si suboxides at the IGO/ SiO_2 interface. These trends have been shown in several other reports as well.^{59,60} Bai et al.⁵⁹ reported that a 760 °C annealing step

Table I. Summary of the measured reference and heterostructure peaks for SiO₂ on (In_xGa_{1-x})₂O₃ (eV) before and after annealing at 600 °C for 5 min in N₂ ambient.

Indium Concentration	Reference (In _x Ga _{1-x}) ₂ O ₃			Reference SiO ₂			Thin SiO ₂ on (In _x Ga _{1-x}) ₂ O ₃					
							As Deposited		Annealed at 450 °C		Annealed at 600 °C	
	Core Level Peak (In 3d _{5/2})	VBM	Core - VBM	Core Level Peak (Si 2p)	VBM	Core - VBM	Δ Core Level (In 3d _{5/2} - Si 2p)	Valence Band Offset	Δ Core Level	VBO	Δ Core Level	VBO
(In _{0.25} Ga _{0.75}) ₂ O ₃	444.65	2.50	442.15	103.40	4.80	98.6	341.6	1.95	341.95	1.6	341.9	1.65
(In _{0.42} Ga _{0.58}) ₂ O ₃	444.40	2.25	442.15	—	—	—	341.45	2.1	341.9	1.65	341.9	1.65
(In _{0.60} Ga _{0.40}) ₂ O ₃	444.35	2.25	442.10	—	—	—	341.3	2.2	341.7	1.8	341.65	1.85
(In _{0.74} Ga _{0.26}) ₂ O ₃	444.20	2.10	442.10	—	—	—	341.2	2.3	341.55	1.95	341.5	2

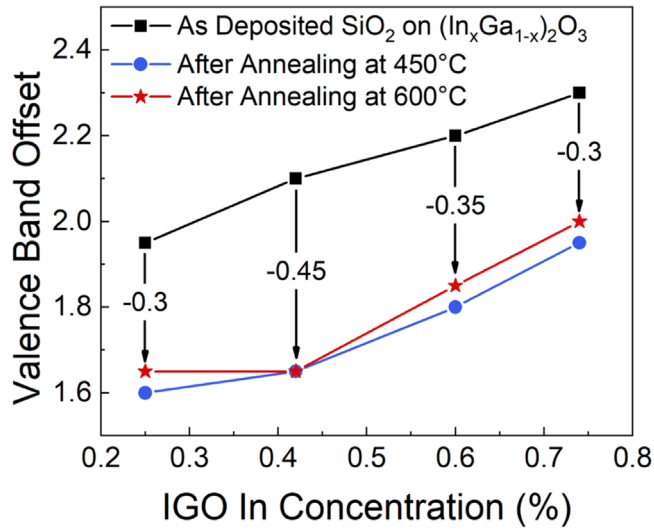


Figure 5. Valence band offsets for the as-deposited and annealed $\text{SiO}_2/(\text{In}_x\text{Ga}_{1-x})_2\text{O}_3$ heterostructures as a function of indium concentration.

causes an interdiffusion layer between a $\text{Ga}_2\text{O}_3/\text{SiO}_2$ interface, also evident in XPS spectra. Table I lists the reference and heterostructure peak locations before and after both annealing steps. The valence band offsets increased after 450 °C annealing for all studied In compositions but showed little additional change after the further 600 °C annealing.

For the ALD deposited thick SiO_2 and reference $(\text{In}_x\text{Ga}_{1-x})_2\text{O}_3$ sample, the elemental peak locations and valence band maximum values remained constant after both annealing steps. The valence band maximum (VBM) was determined by finding the intersection between the linear fits of the flat energy band distribution and leading edge of the valence band from high resolution XPS scans.⁵⁷ For the $(\text{In}_x\text{Ga}_{1-x})_2\text{O}_3$ reference samples, the valence band maxima are 2.5 ± 0.15 eV for $(\text{In}_{0.25}\text{Ga}_{0.75})_2\text{O}_3$, 2.25 ± 0.15 eV for $(\text{In}_{0.42}\text{Ga}_{0.58})_2\text{O}_3$, 2.25 ± 0.15 eV for $(\text{In}_{0.60}\text{Ga}_{0.40})_2\text{O}_3$, and 2.10 ± 0.15 eV for $(\text{In}_{0.74}\text{Ga}_{0.26})_2\text{O}_3$. After measuring the VBMs of the reference samples along with the core delta regions of the $\text{SiO}_2/(\text{In}_x\text{Ga}_{1-x})_2\text{O}_3$ heterostructures, the valence band and conduction band offset can be calculated.^{60–62} The potential deviation in the overall valence band offset was determined by combining the error bars in different binding energies. The valence band offsets for the SiO_2 on $(\text{In}_x\text{Ga}_{1-x})_2\text{O}_3$ before annealing are 1.95 ± 0.30 eV for $(\text{In}_{0.25}\text{Ga}_{0.75})_2\text{O}_3$, 2.10 ± 0.30 eV for $(\text{In}_{0.42}\text{Ga}_{0.58})_2\text{O}_3$, 2.20 ± 0.30 eV for $(\text{In}_{0.60}\text{Ga}_{0.40})_2\text{O}_3$, and 2.30 ± 0.35 eV for $(\text{In}_{0.74}\text{Ga}_{0.26})_2\text{O}_3$.

The change in valence band offsets after annealing the $\text{SiO}_2/(\text{In}_x\text{Ga}_{1-x})_2\text{O}_3$ heterostructures at 450 °C and 600 °C is shown in Fig. 5. After annealing at 450 °C, the change in the band alignment was between 0.3 and 0.45 eV for all compositions studied. After 600 °C annealing, the band alignment remained essentially the same as the 450 °C annealed values across the entire composition range. The shift shown in this study is fairly constant as a function of composition in the $(\text{In}_x\text{Ga}_{1-x})_2\text{O}_3$ and is likely to be due to changes in interfacial chemistry between the SiO_2 and $(\text{In}_x\text{Ga}_{1-x})_2\text{O}_3$, with the change in chemical composition and dipole formation leading to changes in valence band offset, as commonly reported in other systems.^{45–50} TEM of the annealed $(\text{In}_x\text{Ga}_{1-x})_2\text{O}_3$ showed changes in crystallinity that were more pronounced for Ga-rich compositions, but it is the interfacial bonding that controls the band offsets. It is worth noting that crystallinity differences along with the diversification of sub-oxides after annealing may contribute to slight error within the final band alignment measurements. Due to the lack of band alignment studies on Indium based Ga_2O_3 , additional work should be completed to fully understand this material system.

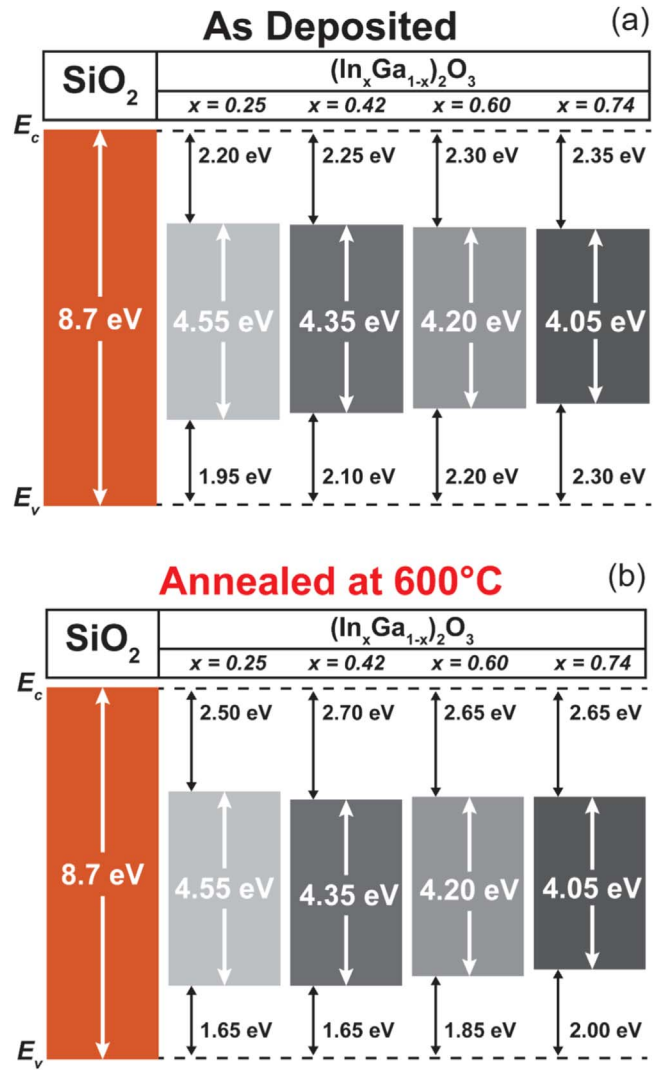


Figure 6. Band diagrams for the $\text{SiO}_2/(\text{In}_x\text{Ga}_{1-x})_2\text{O}_3$ heterostructure (a) as deposited and (b) after annealing at 600 °C for 5 min in N_2 ambient.

The band diagrams for the $\text{SiO}_2/(\text{In}_x\text{Ga}_{1-x})_2\text{O}_3$ heterostructures before annealing (a) and after 600 °C annealing for 5 min in N_2 ambient (b) are shown in Fig. 6. For the as-deposited samples, the SiO_2 has large offsets in both the valence band and conduction band. Figure 6b shows a slight shift in band alignment in all the heterostructure examined after the 600 °C anneal. Despite the shift in the offset, the confinement is still type I and greater than 1 eV for all compositions studied. These offsets allow for good carrier confinement at all compositions of $(\text{In}_x\text{Ga}_{1-x})_2\text{O}_3$ and reinforce the acceptable thermal stability of SiO_2 as a potential dielectric for this material system.

Conclusions

$\text{SiO}_2/(\text{In}_x\text{Ga}_{1-x})_2\text{O}_3$ heterostructures over a range of In concentrations ($x = 0.25–0.74$) were annealed at 450 °C and 600 °C to determine the thermal stability of SiO_2 as a dielectric to IGO. After annealing at 450 °C, the valence band offset shifted between 0.3 to 0.45 eV across the entire In composition range studied. After the 450 °C anneal, the same samples were annealed again at 600 °C and showed no significant change in band alignment to the 450 °C annealed values. The decrease in VBO after 600 °C from the initial values is -0.3 eV for $(\text{In}_{0.25}\text{Ga}_{0.75})_2\text{O}_3$, -0.45 eV for $(\text{In}_{0.42}\text{Ga}_{0.58})_2\text{O}_3$, -0.35 eV for $(\text{In}_{0.60}\text{Ga}_{0.40})_2\text{O}_3$, and -0.3 eV $(\text{In}_{0.74}\text{Ga}_{0.26})_2\text{O}_3$. Even after the

anneals, the band alignment is type I across the full composition range studied. Future work should be done to determine interface state densities of common dielectrics on $(\text{In}_x\text{Ga}_{1-x})_2\text{O}_3$ before and after annealing.

Acknowledgments

The project or effort depicted was also sponsored by the Department of the Defense, Defense Threat Reduction Agency, HDTRA1-17-1-011, monitored by Jacob Calkins and also by NSF DMR 1856662 (Tania Paskova). Research at NRL was supported by the Office of Naval Research, partially under Award Number N00014-15-1-2392. The authors at Leipzig thank Jörg Lenzner for EDX measurements and Monika Hahn for PLD target preparation. Research at NRL was supported by the Office of Naval Research, partially under Award Number N00014-15-1-2392. M.K. acknowledges support by the European Social Fund within the Young Investigator Group “Oxide Heterostructures” (SAB 100310460) and the Leipzig School for Natural Sciences BuildMoNa.

ORCID

S. J. Pearton  <https://orcid.org/0000-0001-6498-1256>

References

- M. Higashiwaki et al., *Appl. Phys. Lett.*, **108**, 133503 (2016).
- Z. Hu et al., *Appl. Phys. Lett.*, **113**, 122103 (2018).
- M. J. Tadjer et al., *J. Electron. Mater.*, **45**, 2031 (2016).
- A. J. Green et al., *IEEE Electron Dev. Lett.*, **38**, 790 (2017).
- M. Higashiwaki and G. H. Jessen, *Appl. Phys. Lett.*, **112**, 060401 (2018).
- M. A. Mastro, A. Kuramata, J. Calkins, J. Kim, F. Ren, and S. J. Pearton, *ECS J. Solid State Sci. Technol.*, **6**, P356 (2017).
- H. von Wenckstern, *Adv. Electron. Mater.*, **3**, 1600350 (2017).
- S. J. Pearton, J. Yang, P. H. Cary, F. Ren, J. Kim, M. J. Tadjer, M. A. Mastro, and P. H. Cary IV, *Appl. Phys. Rev.*, **5**, 011301 (2018).
- S. Rafique, L. Han, A. T. Neal, S. Mou, M. J. Tadjer, R. H. French, and H. Zhao, *Appl. Phys. Lett.*, **109**, 132103 (2016).
- K. Zeng and U. Singiseti, *Appl. Phys. Lett.*, **111**, 122108 (2017).
- J. Bae, H. W. Kim, I. H. Kang, G. Yang, and J. Kim, *Appl. Phys. Lett.*, **112**, 122102 (2018).
- C. Kranert, J. Lenzner, M. Jenderka, M. Lorenz, H. Von Wenckstern, R. Schmidt-Grund, and M. Grundmann, *J. Appl. Phys.*, **116**, 013505 (2014).
- F. Zhang, H. Li, M. Arita, and Q. Guo, *Opt. Mater. Express*, **7**, 3769 (2017).
- X. Wang, Z. Chen, K. Saito, T. Tanaka, M. Nishio, and Q. Guo, *J. Alloys Compd.*, **690**, 287 (2017).
- Y. Kokubun, T. Abe, and S. Nakagomi, *Phys. Status Solidi*, **207**, 1741 (2010).
- M. Grundmann, H. Frenzel, A. Lajn, M. Lorenz, F. Schein, and H. von Wenckstern, *Phys. Status Solidi*, **207**, 1437 (2010).
- F. Zhang, K. Saito, T. Tanaka, M. Nishio, and Q. Guo, *Solid State Commun.*, **186**, 28 (2014).
- F. Zhang, K. Saito, T. Tanaka, M. Nishio, and Q. Guo, *J. Alloys Compd.*, **614**, 173 (2014).
- M. Kneiß, P. Storm, G. Benndorf, M. Grundmann, and H. von Wenckstern, *ACS Comb. Sci.*, **20**, 643 (2018).
- H. Von Wenckstern, Z. Zhang, F. Schmidt, J. Lenzner, H. Hochmuth, and M. Grundmann, *CrystEngComm*, **15**, 10020 (2013).
- H. von Wenckstern, D. Splith, A. Werner, S. Müller, M. Lorenz, and M. Grundmann, *ACS Comb. Sci.*, **17**, 710 (2015).
- H. Von Wenckstern, D. Splith, M. Purfürst, Z. Zhang, C. Kranert, S. Müller, M. Lorenz, and M. Grundmann, *Semicond. Sci. Technol.*, **30**, 024005 (2015).
- F. Fuchs and F. Bechstedt, *Phys. Rev. B—Condens. Matter Mater. Phys.*, **77**, 155107 (2008).
- G. Patzke and M. Binnewies, *Solid State Sci.*, **2**, 689 (2000).
- R. Schmidt-Grund, C. Kranert, T. Böntgen, H. Von Wenckstern, H. Krauß, and M. Grundmann, *J. Appl. Phys.*, **116**, 053510 (2014).
- H. von Wenckstern, in *Gallium Oxide* (Elsevier, Amsterdam) p. 119 (2019).
- M. B. Maccioni and V. Fiorentini, *Appl. Phys. Express*, **9**, 041102 (2016).
- H. Peelaers, D. Steiauf, J. B. Varley, A. Janotti, and C. G. Van De Walle, *Phys. Rev. B—Condens. Matter Mater. Phys.*, **92**, 085206 (2015).
- Z. Zhang, H. Von Wenckstern, J. Lenzner, M. Lorenz, and M. Grundmann, *Appl. Phys. Lett.*, **108**, 123503 (2016).
- M. Baldini, M. Albrecht, D. Gogova, R. Schewski, and G. Wagner, *Semicond. Sci. Technol.*, **30**, 024013 (2015).
- P. Vogt and O. Bierwagen, *APL Mater.*, **4**, 086112 (2016).
- T. Oshima and S. Fujita, *Phys. Status Solidi*, **5**, 3113 (2008).
- Z. Feng et al., *J. Alloys Compd.*, **745**, 292 (2018).
- C. Fares, F. Ren, E. Lambers, D. C. Hays, B. P. Gila, and S. J. Pearton, *J. Vac. Sci. Technol. B*, **36**, 061207 (2018).
- K. Zeng, Y. Jia, and U. Singiseti, *IEEE Electron Device Lett.*, **37**, 906 (2016).
- Z. Feng, Q. Feng, J. Zhang, X. Li, F. Li, L. Huang, H.-Y. Chen, H.-L. Lu, and Y. Hao, *Appl. Surf. Sci.*, **434**, 440 (2018).
- Y. Jia, K. Zeng, J. S. Wallace, J. A. Gardella, and U. Singiseti, *Appl. Phys. Lett.*, **106**, 102107 (2015).
- K. Kita, E. Suzuki, and Q. Mao, *ECS Trans.*, **92**, 59 (2019).
- N. A. Moser, J. P. McCandless, A. Crespo, K. D. Leedy, A. J. Green, E. R. Heller, K. D. Chabak, N. Peixoto, and G. H. Jessen, *Appl. Phys. Lett.*, **110**, 143505 (2017).
- J. Yang et al., *Appl. Phys. Lett.*, **114**, 232106 (2019).
- C. Joishi, Y. Zhang, Z. Xia, W. Sun, A. R. Arehart, S. Ringel, S. Lodha, and S. Rajan, *IEEE Electron Device Lett.*, **40**, 1241 (2019).
- M. Xian, C. Fares, F. Ren, B. P. Gila, Y.-T. Chen, Y.-T. Liao, M. Tadjer, and S. J. Pearton, *J. Vac. Sci. Technol. B*, **37**, 061201 (2019).
- M. Xian, R. Elhassani, C. Fares, F. Ren, M. Tadjer, and S. J. Pearton, *J. Vac. Sci. Technol. B*, **37**, 061205 (2019).
- H. Zhou, S. Alghamdi, M. Si, G. Qiu, and P. D. Ye, *IEEE Electron Device Lett.*, **37**, 1411 (2016).
- M. K. Yadav, A. Mondal, S. Das, S. K. Sharma, and A. Bag, *J. Alloys Compd.*, **819**, 153052 (2020).
- S. Y. Chiam, W. K. Chim, Y. Ren, C. Pi, J. S. Pan, A. C. H. Huan, S. J. Wang, and J. Zhang, *J. Appl. Phys.*, **104**, 063714 (2008).
- N. V. Nguyen, M. Xu, O. A. Kirillov, P. D. Ye, C. Wang, K. Cheung, and J. S. Suehle, *Appl. Phys. Lett.*, **96**, 052107 (2010).
- L. Sun, H.-L. Lu, H.-Y. Chen, T. Wang, X.-M. Ji, W.-J. Liu, D. Zhao, A. Devi, S.-J. Ding, and D. W. Zhang, *Nanoscale Res. Lett.*, **12**, 102 (2017).
- H. H. Wei, G. He, X. S. Chen, J. B. Cui, M. Zhang, H. S. Chen, and Z. Q. Sun, *J. Alloy and Compounds*, **591**, 240 (2014).
- W. F. Lim and K. Y. Cheong, *MRS Proc.* 1433 (2012), Mrss12–1433-h04–02.
- Y. Hu, C. Wang, H. Dong, R. M. Wallace, K. Cjho, and W.-H. Wang, *ACS Appl. Mat. Interfaces*, **8**, 7595 (2016).
- M. Kneiß, A. Hassa, D. Splith, C. Sturm, H. Von Wenckstern, T. Schultz, N. Koch, M. Lorenz, and M. Grundmann, *APL Mater.*, **7**, 101102 (2019).
- A. Hassa, H. Von Wenckstern, D. Splith, C. Sturm, M. Kneiß, V. Prozheeva, and M. Grundmann, *APL Mater.*, **7**, 022525 (2019).
- M. Lorenz et al., *Laser Chem.*, **2010**, 140976 (2010).
- C. Fares, M. Kneiß, H. von Wenckstern, M. Grundmann, M. Tadjer, F. Ren, E. Lambers, and S. J. Pearton, *APL Mater.*, **7**, 071115 (2019).
- C. Fares, M. Kneiss, H. von Wenckstern, M. Grundmann, M. J. Tadjer, F. Ren, D. Hays, B. P. Gila, and S. J. Pearton, *ECS Trans.*, **92**, 79 (2019).
- E. A. Kraut, R. W. Grant, J. R. Waldrop, and S. P. Kowalczyk, *Phys. Rev. Lett.*, **44**, 1620 (1980).
- D. C. Hays, B. P. Gila, S. J. Pearton, A. Trucco, R. Thorpe, and F. Ren, *J. Vac. Sci. Technol.*, **35**, 011206 (2017).
- B. Bai et al., *Chin. Phys. B*, **28**, 106802 (2019).
- A. Thogerson, J. H. Selij, and S. Marstein, *J. Electrochem. Soc.*, **159**, D276 (2012).
- M. Perego and G. Seguin, *J. Appl. Phys.*, **110**, 053711 (2011).
- M. T. Nichols, W. Li, D. Pei, G. A. Antonelli, Q. Lin, S. Banna, Y. Nishi, and J. L. Shohet, *J. Appl. Phys.*, **115**, 094105 (2014).